Hindawi
Journal of Advanced Transportation
Volume 2023, Article ID 9892819, 1 page
https://doi.org/10.1155/2023/9892819

Retraction

Retracted: Research on Separation and Emission Reduction of Regional Airliner Based on Wake Encounter Response Model

Journal of Advanced Transportation

Received 12 December 2023; Accepted 12 December 2023; Published 13 December 2023

This article has been retracted by Hindawi, as publisher, following an investigation undertaken by the publisher [1]. This investigation has uncovered evidence of systematic manipulation of the publication and peer-review process. We cannot, therefore, vouch for the reliability or integrity of this article.

Please note that this notice is intended solely to alert readers that the peer-review process of this article has been compromised.

Wiley and Hindawi regret that the usual quality checks did not identify these issues before publication and have since put additional measures in place to safeguard research integrity.

We wish to credit our Research Integrity and Research Publishing teams and anonymous and named external researchers and research integrity experts for contributing to this investigation.

The corresponding author, as the representative of all authors, has been given the opportunity to register their agreement or disagreement to this retraction. We have kept a record of any response received.

References

[1] W. Pan, H. Wang, Y. Luo, J. Wang, and S. Han, "Research on Separation and Emission Reduction of Regional Airliner Based on Wake Encounter Response Model," *Journal of Advanced Transportation*, vol. 2022, Article ID 3584461, 16 pages, 2022.

Hindawi
Journal of Advanced Transportation
Volume 2022, Article ID 3584461, 16 pages
https://doi.org/10.1155/2022/3584461

Research Article

Research on Separation and Emission Reduction of Regional Airliner Based on Wake Encounter Response Model

Weijun Pan, Hao Wang, Yuming Luo, Jingkai Wang, and Shuai Han

College of Air Traffic Management, Civil Aviation Flight University of China, Deyang 618307, China

Correspondence should be addressed to Weijun Pan; wjpan@cafuc.edu.cn

Received 4 March 2022; Revised 5 May 2022; Accepted 18 May 2022; Published 4 August 2022

Academic Editor: Muhammad Arif

To ensure the safety of aircraft operation, the current regional passenger aircraft maintains a large distance from the preceding aircraft in actual operation, which result in reducing the operation efficiency of airports and airspace, and increasing pollutant emissions. To address these issues, in this paper, two aircraft types are selected in which the CRJ-900 encounters the trailing wake vortices of the A380 in front. An improved strip model is developed to build the CRJ-900 overall response wake encounter value. First, the safety of the CRJ-900 longitudinal and lateral wake encounters in different flight stages is analyzed. Second, we calculate the critical safety separation and its impact on air transport efficiency. Third, we use the LTO model to measure the reduction of aircraft fuel consumption and pollutant emissions. The results demonstrated that the medium-sized aircraft CRJ-900 has the potential to reduce the wake separation when following the super-heavy A380 aircraft. In terms of the critical safety separation calculated by the safety index, the operating efficiency of airports and airspace could be effectively improved, allowing the reduction of pollutant emissions during aircraft take-off and landing. During the takeoff, level flight, and landing phase, the results are summarized as follows: when the CRJ-900 is 13km away from the A380, the maximum lift variation is 11334N, 8157N, and 7366N; the maximum rolling moment variation is 43836N•M, 35274 N•M, and 28487 N•M; the maximum value of the rolling moment coefficient (RMC) is 0.0171, 0.0160, and 0.0130; when the RMC critical value is 0.031, the maximum safe separation for different flight stages is 11960m, which is 1040m shorter than the existing separation; when the RMC critical value is 0.05, the maximum safe separation distance of each stage is 10083m, a reduction of 2917m compared with the existing separation; when the RMC threshold is 0.07, the maximum safe separation of different flight stages is 9021m, a reduction of 3979m compared to the existing separation; when the RMC value is between 0.031-0.07, the fuel consumption can be reduced by 7.9%–12.8%, and the pollutant emission can be reduced by 9.1%–12.8%.

1. Background

Wake vortex is a by-product of aircraft lift, which affects the safety of aircraft operation. In particular, the wake generated by super-heavy aircraft has the characteristics of large initial circulation, long transmission distance, and long duration, which may bring safety hazards to the trailing aircraft. In practice, the design of regional airliners is different from that of conventional airliners. At the same time, the impact of the aircraft wake in front on the regional airliners is still unknown, yielding a large approach and take-off interval used by airports during the control process. That will result in low runway utilization and limit the capacity of controlled airspace, also increase fuel consumption and pollutant emissions. To achieve the purpose of energy saving and emission reduction, it is necessary to study and analyze the safety of the wake vortex that encountered on the regional airliner, allowing for the reduction of the wake interval and the improvement of the control operation efficiency.

The outline of this paper is shown in Figure 1. First, the models of wake generation and evolution were analyzed, and different models of wake-induced velocity were compared to determine the mathematical model of wake dissipation. Second, we analyzed the possible scenarios of wake encounters in different flight stages, and the aerodynamic response model of the aircraft's overall wake encounters was

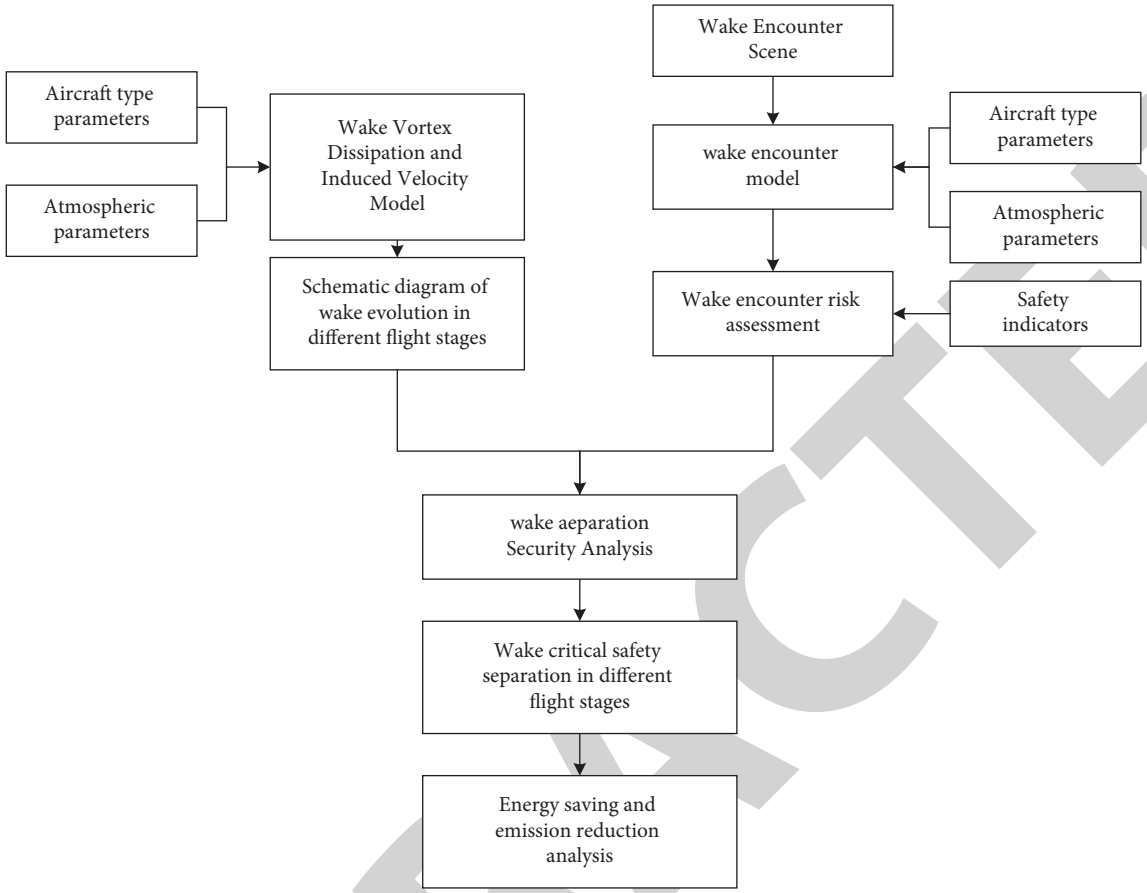

Figure 1: The framework of this research.

constructed. Finally, to study the impact on energy saving and emission reduction under this separation, we selected the appropriate safety index and analyzed the safety of wake encounter, and also calculated the critical safety separation of wake in different flight stages according to the limit value of rolling moment coefficient.

2. Literature Review

Based on the research ideas of this paper, the research status of wake generation, evolution, and wake encounter is summarized.

The generation and development of aircraft wake is related to factors such as aircraft configuration and atmospheric environment. The atmospheric environment is unpredictable, and the evolution and dissipation of the wake also changes, which is difficult to predict. Experts and scholars have carried out a lot of research on this.

For the study of wake generation and subsequent encounter, Crow conducted a large number of observations and experiments in the 1970s to study the generation and dissipation mechanism of approach wake [1]; NASA Langley Research Center analyzed the effects of turbulence and Reynolds number on the motion and attenuation of wake vortex in the atmospheric environment, and established the first wake dissipation model [2].

Luton et al. [3] used numerical simulation technology to study the wake evolution in the near-earth stage, and found that the mutual induction between the wake vortex and its mirror vortex would cause Crow instability; Sarpkaya [4] used numerical simulation and by means of the detection experiment at Memphis Airport; the simulation and measurement data were compared, and a new wake dissipation model was established on the basis of the Green model to predict the wake dissipation in the real atmospheric environment [5]; at the same time, this model has been used in the Aircraft Vortex Spacing System developed by NASA [6]; Proctor and Han [7] used the three-dimensional large eddy simulation method to study the influence of ground effects on wake dissipation. It was shown that the ground effect will affect the wake vortex trajectory and descent rate at a height of about 3 times the initial vortex core spacing. When the vortex core drops to 0.6 times the initial vortex core spacing from the ground, the ground effect will rapidly reduce the wake intensity; Robins et al. [8] proposed an algorithm for predicting the trajectory and intensity decay of aircraft trailing vortices and used a database to compare the algorithm prediction and measurement data; Holzäpfel [9–11] comprehensively considered the effects of turbulence, atmospheric formation, and wind on wake dissipation, and proposed a two-stage wake dissipation model

to represent the dissipation of the entire wake vortex field, and this model has been used in the Wake Vortex Advisory System; Proctor et al. [12] proposed a wake for real-time prediction of wake transmission and intensity attenuation tass driven algorithm for wake prediction, which takes into account the influence of meteorological factors on wake evolution; at the same time, through the research method of large eddy simulation, a three-stage wake dissipation model was proposed on the basis of the two-stage wake dissipation model [13]; [14]; Breitsamter [15] explained the wake from near-field to far-field by combing wake research projects, models, flight experiments, and numerical simulations. In the same year, Hennemann and Holzäpfel [16] conducted a large eddy simulation of the wake evolution under different atmospheric conditions, and analyzed the influence of turbulence level and temperature split on wake generation and evolution; De Visscher et al. [17] considered the influence of wind (crosswind and headwind components) on wake transport dissipation and developed a rapid prediction of wake behavior; the software could predict in real time the time evolution of the wake vortex generated by the evolution of a given aircraft under given environmental meteorological conditions; the influence of terrain changes on wake dissipation was studied, and plate-like lines were added on the ground to achieve accelerated wake dissipation [18, 19]; the dissipation of near ground wake can be studied by lidar detection [20, 21].

The formulation of wake separation standard not only considers the dissipation of wake in the atmospheric environment but also needs to consider the resistance of aircraft when encountering wake. Therefore, it is of great research significance to evaluate the safety of wake encountering. NASA obtains wake dissipation and aircraft response data in the actual atmospheric environment through actual flight experiments, and establishes a wake encounter database [22]; Netherlands Aerospace Center has developed wake (wake vortex induced risk assessment) for S-wake, ATC wake, and I-wake projects to evaluate the safety of reduced separations [23, 24]; The safety assessment of wake encounter severity can be reflected by the required angular velocity [25], maximum roll angle velocity [26], roll moment coefficient [27], wake encounter roll control ratio [28], wake vortex kinetic energy and vortex resistance when the roll torque and damping torque are turned parallel [28] WSVS is used to study the aircraft type pairing, main weather conditions, and the resulting wake vortex behavior. It is found that the great potential of safely reducing aircraft spacing mainly exists in sufficiently strong crosswind conditions [29] by comprehensively considering the final approach track, the influence of crosswind, and the wake bearing capacity of rear aircraft, an optimization model of wake separation under paired approach is established [20, 30].

With regard to the research on aircraft pollutant emission, the International Civil Aviation Organization [31] established the model emission database and used the standard takeoff and landing cycle to calculate the pollutant emission of aircraft below 1000 m in different flight stages within the airport; based on the ICAO emission model, the pollutant emission estimation during thrust reduction is studied by using discrete data [32]; The Federal Aviation Administration has developed sage (Global airspace aviation emission assessment system); Boeing proposed BM2 method to modify the ICAO model and estimate the pollutant emission in actual flight more accurately; based on ICAO database, BM2 model, and basic aircraft data (Bada), European Air Traffic Control Agency developed advanced emission model to estimate actual pollutant emissions through 4D track data (Euro control); Cook et al. studied the weight relationship between different pollutants, obtained the concept of dynamic cost index covering emission cost, and used it for flight delay analysis [33]; the four-dimensional emission database list is established by using ATC track data [34]; Schumann optimized route pollutant emission through wake cloud and fuel consumption [35]; Jiang et al. analyzed the new aircraft ground taxiing mode and study its impact on airport pollutant emission [36]. Combined with the single runway ground taxiing method, the aircraft pollutant emission assessment model of Regional Airport is established [37].

In this paper, by analyzing the generation and dissipation process of tail vortex in different flight stages, the stress model of CRJ-900 encountering wake is established by using the aerodynamic method of strip model. According to the aircraft operation performance and relevant risk safety indicators, the safety of CRJ-900 encountering wake in different flight stages is studied and analyzed. Using the limit value of safety index, the critical safety separation in different flight stages is deduced, its impact on operation efficiency is analyzed, and the reduction of pollutant emission is estimated.

3. Materials and Methods

The wake encounter safety mainly depends on the wake vortex strength of the aircraft generating the wake and the response of the follower aircraft when encountering the wake. Therefore, it is necessary to study the wake vortex characteristics, dissipation, and the response model of the wake encounter.

3.1. Wake Dissipation Model. In the initial dissipation stage, the strength of the wake decreases mainly by itself, so the dissipation speed is slow; the time for the wake vortex to enter the fast dissipation stage is related to the dimensionless vortex dissipation rate; the calculation formula of wake vortex entering fast dissipation time t_w is as follows:

$$\begin{cases} t_w = t_z\left(\dfrac{0.7475}{\varepsilon^*}\right)^{0.75}, & \varepsilon^* \geq 0.2535, \\ t_w\varepsilon^* = \left(\dfrac{t_w}{t_z}\right)^{0.25} e^{\left(\dfrac{-0.7t_w}{t_z}\right)}, & 0.0121 \leq \varepsilon^* \leq 0.2535, \\ t_w = t_z\left(9.18 - 180\varepsilon^*\right), & 0.001 \leq \varepsilon^* \leq 0.0121, \\ t_w = 9t_z, & \varepsilon^* < 0.001, \end{cases} \quad (1)$$

where t_w is the time to start the rapid dissipation phase, t_z is the characteristic time, and its calculation formula is

$$t_z = \frac{b_x}{v_x}, \quad (2)$$

where b_x is the initial wake distance and v_x is the initial characteristic velocity of the wake.

ε^* is the eddy dissipation rate, and its calculation formula is as follows:

$$\varepsilon^* = \frac{\left(\varepsilon b_x\right)^{1/3}}{v_x} = \frac{2\pi b_x\left(\varepsilon b_x\right)^{1/3}}{\Gamma_x} = \frac{\pi^2\rho V B b_x\left(\varepsilon b_x\right)^{1/3}}{2mg}, \quad (3)$$

where ε is the turbulent dissipation rate, and the calculation formula is as follows:

$$\varepsilon = \frac{C_{mu}^{0.75}k^{1.5}}{l}, \quad (4)$$

where $C_{mu} = 0.09$ is a constant, k is the turbulent kinetic energy, and l is the characteristic scale of turbulence.

By calculating the wake duration in the near-field region and comparing it with the time of CRJ-900 encountering wake, we can determine whether CRJ-900 is encountering near-field wake or far-field wake.

$$\begin{aligned} \Gamma_x &= \frac{4Mg}{\rho\pi BV}, \\ b_x &= \frac{\pi}{4}B, \\ r_x &= 5.2\%b_x, \end{aligned} \quad (5)$$

where M is the weight of the aircraft, g is the acceleration of gravity, B is the wingspan of the aircraft, and V is the flight speed of the aircraft.

Based on the AVOSS system, NASA has developed an APA model of wake dissipation. The equation is

$$\Gamma^* = \frac{\Gamma}{\Gamma_0} = \exp\left[-\left(C + 0.25N^{*2}\right)\right]\frac{t - t_w}{t_w}, \quad (6)$$

where C is a constant, usually 0.4525; t_w is the time for the wake vortex to enter and dissipate rapidly; $0.25\,N^{*2}$ represents the effect of atmospheric stratification on the dissipation of the wake vortex.

In this paper, A380 aircraft is selected as the aircraft to produce wake vortex for calculation, and the specific model parameters are shown in Table 1.

Through the customs clearance calculation, we can get the dissipation of the wake vortex of A380 in different flight stages under different atmospheric stratification and turbulence degree, as shown in Figure 2. From this, we can know the dissipation of A380 aircraft wake vortex at different time and distance, as shown in Table 2.

3.2. Wake Encounter Analysis. There are three ways for aircraft to enter the wake vortex field of the front aircraft: (1) across the front wake; (2) longitudinal entry into double wake vortex of front aircraft; (3) longitudinal entry into the single vortex of the front aircraft. The details are shown in Figure 3.

3.2.1. Across the front Wake Vortex. When the aircraft crosses the wake vortex of the front aircraft, as shown in mode *a* in Figure 3, it will experience a backward wash up wash down wash up force, which will cause a large turbulence of the aircraft, resulting in a sudden change in the altitude, speed, and attitude of the aircraft. In serious cases, it will cause the aircraft out of control, or even cause a safety accident.

3.2.2. Longitudinal Entry into Double Wake Vortex of front Aircraft. As shown in mode *B* in Figure 3, when entering the double vortex of the front aircraft longitudinally, the aircraft will suddenly drop height due to the influence of downwash air flow. At high altitude, the pilot has enough time to respond to the adjustment;.In the takeoff and approach phase, sudden height drop is easy to cause safety accidents.

3.2.3. Longitudinal Entry into Single Wake Vortex of front Aircraft. When the aircraft enters the center of the single vortex in the wake of the front aircraft, as shown in mode *C* in Figure 3, the two wings are subjected to the upwash force and downwash force, respectively, causing the aircraft to roll. When the roll angle is too large, it will cause the aircraft to lose lift, or even enter the weightlessness state, causing safety accidents.

The velocity field generated by the wake pair when encountering an aircraft is not uniform. The velocity of the flow field varies greatly on the surface of the aircraft, as shown in Figure 4. The classical aerodynamic model suitable for uniform flow field is not suitable for calculating the aerodynamic force and torque generated by flow field, so a distributed aerodynamic model is needed [38]. Standard methods include strip method and lifting surface method. They require the velocity vector of each time step discrete point (generally one point for each aerodynamic section) to be simulated, as shown in Figure 4(b).

In the strip model, the aircraft is simplified as wing, fuselage, horizontal, and vertical tail surfaces. The black lines in Figure 4(b) represent a simplified aircraft model. For each strip element, the angle of attack caused by eddy current is

Table 1: A380 type parameters.

Type	Wingspan (m)	Cruise speed (m/s)	Final approach speed (m/s)	Maximum takeoff/landing weight (kg)	Wing area ($m^{2)}$	Wake classification
A380-800	79.75	290.967	70.993	560000/386000	845	*H*

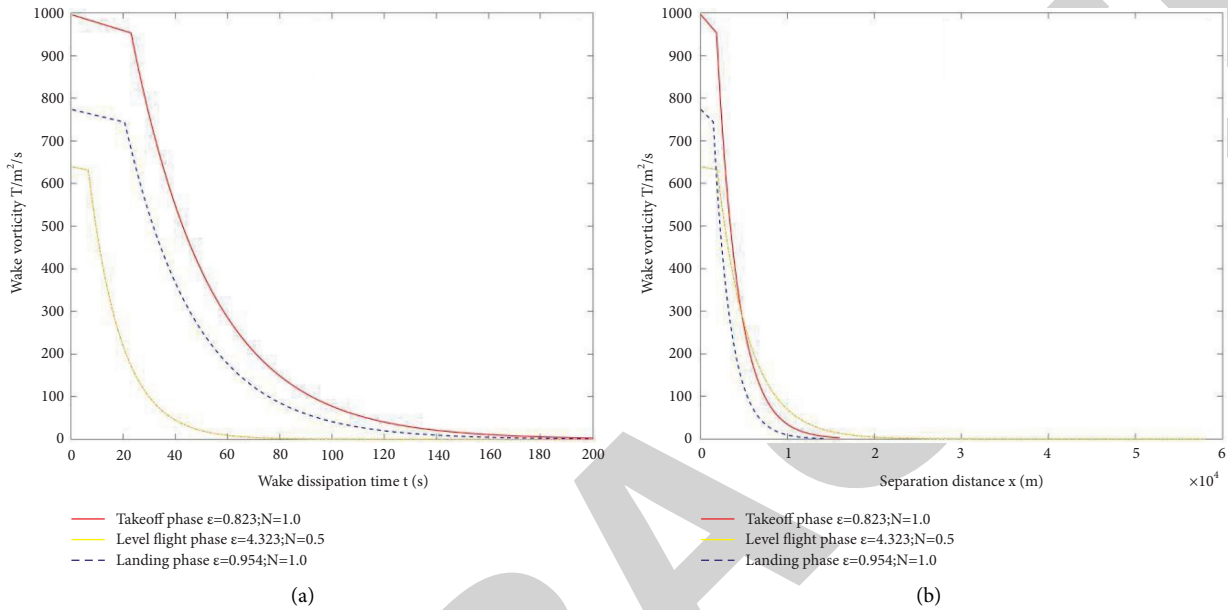

Figure 2: Variation of wake vorticity in different flight stages. (a) Circulation changes with time. (b) Circulation varies with separation distance.

Table 2: A380 wake dissipation parameters.

Flight phase	Γ (m^2/s)	v_x (m^2/s)	t_z (s)	ε ($m^2/s^{4.5}$)	ε^* ($s^{-0.5}$)	t_w (s)	Circulation value at different separation Γ_l (m^2/s)			
							7.4	9.3	11.1	13
Takeoff	1137	2.53	24.75	0.144	0.82	23.26	142.0	70.8	38.0	18.3
Level flight	553	1.41	43.97	6.303	10.88	5.9	71.4	36.5	20.5	10.3
Landing	773	1.96	31.87	0.105	0.95	26.56	101.8	50.9	27.5	13.4

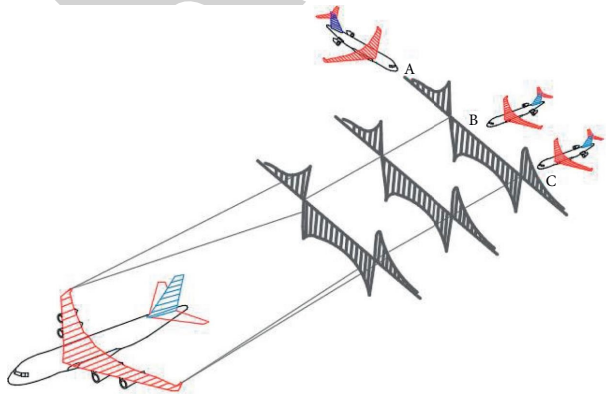

Figure 3: Schematic diagram of different modes of wake vortex field before aircraft entering.

calculated. In order to prevent the local angle of attack from exceeding the maximum angle of attack, the strip model realizes the special limitation of the maximum angle of attack.

3.3. Response Analysis of CRJ-900 Aircraft. When following the front aircraft, the wake of the front aircraft will mainly cause the force change, roll change, and height change of the rear aircraft, while when crossing the wake of the front aircraft, it will mainly cause the force change, pitch change, and height change of the rear aircraft. In this paper, the calculation method of each physical quantity of CRJ-900 encountering wake is given, and the simplified force model of CRJ-900 is given. The parameters of CRJ-900 are shown in Table 3.

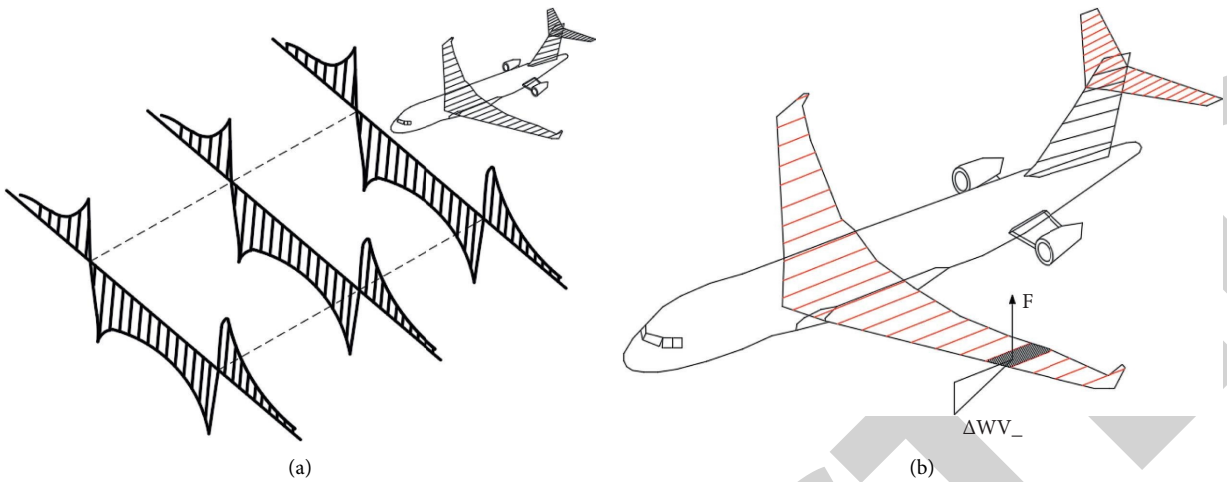

Figure 4: Strip model of wake vortex encountering. (a) Aircraft encountering wake vortex. (b) Discretization of strip method and local airspeed.

Table 3: Geometric main dimensions of CRJ-900-700 aircraft.

Wingspan (m)	Wing area (m^2/s)	Maximum takeoff weight (kg)	Maximum landing weight (kg)	Cruise altitude (m)	Cruise speed (m/s)
24.85	70.61	36504	33340	12496	245.83

3.3.1. Aircraft Lift. The calculation of wing lift variation is shown in formulas (7) and (8):

$$\Delta L = \frac{1}{2}\rho V^2 \int_{-B/2}^{B/2} C_l'(y)\mathrm{CL}(y)\mathrm{d}y, \tag{7}$$

where ΔL is the lift variation, $C_l'(y)$ is the lift coefficient variation, $\mathrm{CL}(y)$ is the spanwise coordinate of the aircraft wing, and y is the chord length. The lift variation of aircraft is mainly caused by the wing, so only the lift variation of the wing is considered when calculating the lift variation in this paper.

$$C_\mathrm{l}'(y) = f\Delta\alpha(y) = \mathrm{f}\arctan\left[\frac{V_\mathrm{v}(y)}{V}\right] \approx f\frac{V_\mathrm{v}(y)}{V}, \tag{8}$$

where f is the lift line slope, $\Delta\alpha(y)$ is the angle of attack variation of the wing section, and $V_\mathrm{v}(y)$ is the induced velocity of the wake field on the wing section.

According to the momentum theorem, the calculation method of the force on any part of the body when encountering the wake is given in equation (9) as follows:

$$F = \rho \mathrm{S}V_v(y)^2, \tag{9}$$

where F is the force on any part of the aircraft body and S is the projected area of any part of the aircraft.

3.3.2. Calculation of Rolling Moment. The calculation of wake induced torque revolves around the basic principle of torque, that is, a force multiplied by a certain distance (torque arm). Therefore, for the wing, the rolling moment generated only by the wake is expressed as follows:

$$Z = D \times F, \tag{10}$$

where Z is the rolling moment generated by the wake vortex, D is the position of a certain point on the wing from the center of the wing, and F is the induced rolling force of the wake vortex, which is equal to the lift of the aircraft changed by the wake vortex.

Because the position of the following aircraft entering the front engine's wake is uncertain, the maximum induced torque can be obtained by the strip model, and the safety analysis can be carried out according to the maximum induced torque.

Based on the strip method (Figure 5), this paper calculates the lift variation caused by the wake vortex on a strip and then obtains the induced torque on the strip.

$$\begin{aligned} d\Gamma(x) &= \frac{1}{2}\rho V_r^2 fl(x) f(x)\Delta\beta(x)\mathrm{d}x, \\ \Delta Zv &= d\Gamma(x)\cdot x = \frac{1}{2}\rho V_r^2 fl(x) f(x)\Delta\beta(x)x\mathrm{d}x, \end{aligned} \tag{11}$$

where $d\Gamma(x)$ is the local lift variation; ΔZ_v is the local induced moment; V_r is the incoming velocity of the air, which is approximately equal to the flight velocity of the aircraft; $\mathrm{fl}(x)$ is the lift line coefficient at position x; $f(x)$ is the chord length; $\Delta\beta(x)$ is the change in angle of attack.

Because the change of angle of attack is very small, it is approximately equal to

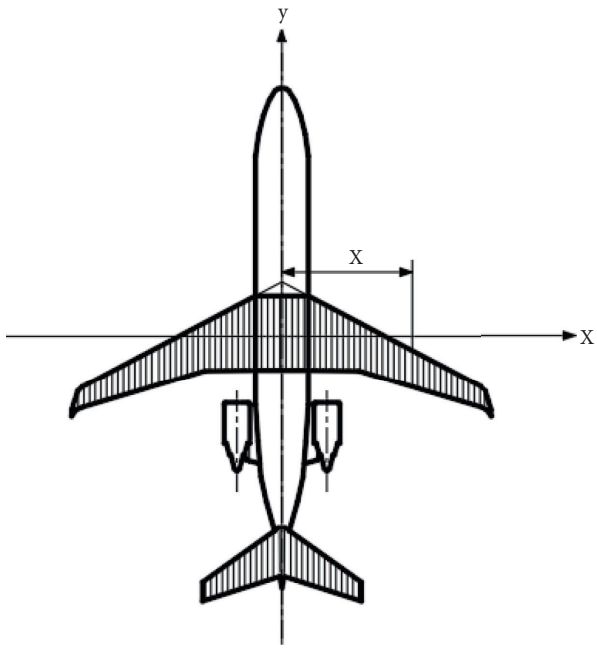

Figure 5: Strip model of CRJ-900 stress calculation.

$$\Delta\beta(x) \approx \frac{V_\theta(x)}{V_f}, \tag{12}$$

where $\Delta\beta(x)$ is the change of angle of attack caused by wake vortex.

After integration, the induced moment Zv of wake vortex to aircraft can be obtained as follows:

$$\mathrm{Zv} = \frac{\rho \mathrm{f} V_f}{2} * \int_{-b_A/2}^{b_A/2} V_\theta(x)\mathrm{f}(\mathrm{x})\mathrm{x}\mathrm{d}x, \tag{13}$$

where $\mathrm{V}_\theta(x)$ is the induced velocity of the front aircraft's wake; f is the slope of the lift line.

As an index to measure the safety of wake encounter [26], the rolling moment coefficient (RMC) can be expressed as

$$\mathrm{RMC} = \frac{\mathrm{Zv}}{1/2\rho V_f^2 \mathrm{S}_f b_\mathrm{f}}, \tag{14}$$

where S_f is the wing area of follow aircraft; b_f is the wingspan of follow aircraft.

At the same time, according to the limit value of aircraft rolling moment coefficient, the maximum rolling moment can be obtained as follows:

$$Zv_{\max} = \frac{1}{2}\mathrm{RMC}_{\max}\rho V_f^2 S_f b_f, \tag{15}$$

where $Zv_{\max}$ is the maximum rolling moment; $\mathrm{RMC}_{\max}$ is the maximum rolling moment coefficient.

3.3.3. Force Model Calculation of Wake Vortex before Crossing. Taking the position of the rear aircraft shown in Figure 6 as an example, the forces on the wing, airframe, engine, and horizontal tail of the rear aircraft are analyzed, respectively.

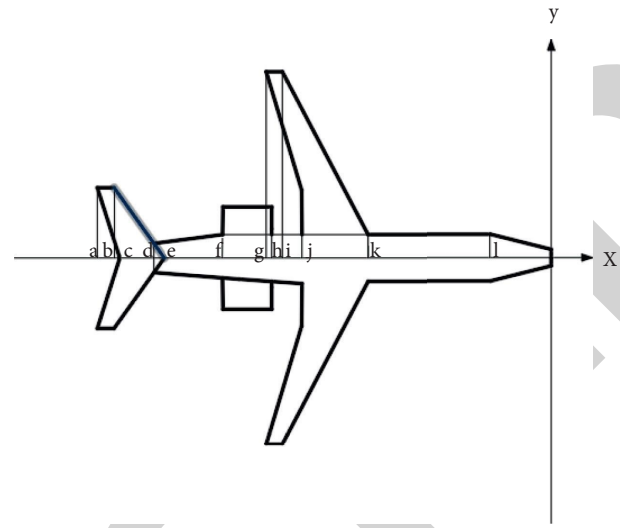

Figure 6: Schematic diagram of stress calculation model of cross wake vortex.

It can be concluded that the stress calculation formula of engine block and engine is as follows:

$$\begin{aligned} F_f = 2\rho\Bigg(& \int_d^f \int_0^{((L/2-D/2)/(e-h))(r-1)+(j/2)} {V_r}^2 \mathrm{d}s\mathrm{d}r \\ & + \int_f^l \int_0^{L/2} {V_r}^2 \mathrm{d}s\mathrm{d}r + \int_l^0 \int_0^{((L/2-M/2)/(0-k))(r-1)+(L/2)} {V_r}^2 \mathrm{d}s\mathrm{d}r \\ & + \int_f^h \int_0^{B_{\mathrm{ET}}/2} {V_r}^2 \mathrm{d}s\mathrm{d}r - \int_f^h \int_0^{H/2} {V_r}^2 \mathrm{d}s\mathrm{d}r \Bigg), \end{aligned} \tag{16}$$

where F_t is the force on the rear fuselage, d is the length of the aircraft fuselage, j is the length of the wing extension line from the fuselage, l is the length of the fuselage, L is the width of the fuselage, M is the width of the fuselage at the fuselage, D is the width of the fuselage d from the fuselage, and h to f are the length of the engine.

The calculation formula of wing downwash force is as follows:

$$\begin{aligned} F_w = 2\rho\Bigg(& \int_\mathrm{i}^k \int_0^{((B/2-K/2)/(i-k))(r-1)+(B/2)} {V_r}^2 \mathrm{d}s\mathrm{d}r \\ & + \int_g^i \int_0^{B/2} {V_r}^2 \mathrm{d}s\mathrm{d}r - \int_g^j \int_0^{((B/2-J/2)/(g-j))(r-1)+(B/2)} {V_r}^2 \mathrm{d}s\mathrm{d}r \\ & - \int_j^k \int_0^{L/2} {V_r}^2 \mathrm{d}s\mathrm{d}r \Bigg), \end{aligned} \tag{17}$$

where F_w is the force on the wing, g to i is the wingtip length, j to k is the wingroot length, B is the wingspan, J is the distance between the trailing edge of the wing and the fuselage axis, and L is the fuselage width.

The shape of the horizontal tail is similar to that of the wing, and the force calculation formula is as follows:

$$F_{ht} = 2\rho\left(\int_b^e \int_0^{((A/2-0)/(b-e))(r-1)+(A/2)} {V_r}^2 \mathrm{d}s\mathrm{d}r + \int_a^b \int_0^{A/2} {V_r}^2 \mathrm{d}s\mathrm{d}r - \int_a^b \int_0^{((A/2-0)/(a-b))(r-1)+(A/2)} {V_r}^2 \mathrm{d}s\mathrm{d}r\right), \tag{18}$$

where F_{ht} is the force on the flat tail, a to b is the tip length of the horizontal tail, c to e is the heel length of the horizontal tail, and A is the span of the horizontal tail.

Therefore, the force exerted on the following aircraft by the wake vortex of the front engine can be obtained according to equation (16), equation (17), and equation (18):

$$F_A = F_w + F_f + F_{ht}, \tag{19}$$

where F_A is the overall force of the aircraft.

3.3.4. Height Change Calculation. When the aircraft encounters the wake, the calculation formula of altitude change is shown in equation (12) as follows:

$$H = \frac{1}{2}\frac{F_A}{M}(t_m + t_n)^2, \tag{20}$$

where H is the descending or ascending height, F_A is the force on the whole aircraft, which can be calculated by equation (20), t_m is the pilot response time, and t_n is the aircraft response time.

3.3.5. Turbulence Intensity. In this paper, the overload increment is used as the criterion to measure the turbulence intensity, and its corresponding turbulence intensity level is shown in the table below. The overload increment is the acceleration of the aircraft flying in the turbulent atmosphere, expressed as a multiple of the gravity acceleration g; the calculation formula is as follows:

$$\Delta n = \frac{F_A}{M_f g}, \tag{21}$$

where M_{f} is the mass of the following aircraft.

3.3.6. Fuel Consumption and Pollutant Emission. The ideal landing and takeoff cycle under international standard atmosphere (ISA) is divided into four stages, and the engine power setting of each stage is different. Table 4 lists the LTO cycles of the CF34-8C5 engine.

The calculation formula of aircraft fuel consumption is

$$\mathrm{F}_c = \sum_{i,j}\left(N_i \times \mathrm{S}_{i,j} \times T_i\right), \tag{22}$$

where N_i is the number of type I aircraft engines; F_i is the working time of type i aircraft in phase j; T_i is the fuel consumption of single engine of model i aircraft (kg/s).

The fuel saving rate is

$$\tau_C = \frac{F_C - F_{C'}}{F_C}. \tag{23}$$

where $F_{C'}$ is the fuel consumption of the aircraft when the calculated safety separation is used.

Pollutant emissions can be calculated as

$$E_k = \sum_{i,j}^{k}\left(N_i \times S_{i,j} \times T_i \times U_{i,k}\right), \tag{24}$$

where $U_{i,k}$ is the emission index of pollutant k in a single engine of type i aircraft.

The pollutant emission reduction rate is

$$\tau_e = \frac{E_k - E_{k'}}{E_k}, \tag{25}$$

where $E_{k'}$ is the pollutant emission when the calculated safety separation is used.

4. Results and Discussion

The most important influence of the wake vortex field on its safety is that its velocity field will change the lift of the aircraft, which in turn will cause changes in the aircraft's flight attitude, resulting in changes in roll, pitch, altitude loss, etc., which will affect the control stability of the aircraft. In order to quantify the response of the aircraft when a wake encounter occurs, the wake encounter model established in Section 3 is used, and the effect of the wake vortex field is introduced to calculate the additional induced force and moment generated by the aircraft wake encounter. The numerical changes of each safety index are used to evaluate the wake encounter risk of the CRJ-900 following the A380 in different flight stages under the RECAT-CN wake separation standard, and give the limit value of the rolling moment coefficient to analyze the critical safety separation of the wake.

4.1. Longitudinal Encounter with Front Wake Vortex. According to the calculation of CRJ-900 longitudinal encounter wake vortex, we can get the changes of aerodynamic characteristics of CRJ-900 aircraft in takeoff, level flight, and landing stages, and analyze the safety of encounter wake vortex. In order to facilitate calculation, the force in this paper is negative in the direction of gravity, negative to the left from the vortex core, and negative in the counterclockwise direction of rolling moment.

4.1.1. Lift Variation. The lift variation of single vortex before longitudinal encounter of CRJ-900 aircraft is shown in Figure 7. The lift variation first increases sharply and then decreases with the distance. In the takeoff and landing stages, the lift is the largest when it is 6.3 m away from the vortex core center, and the lift reaches the maximum at 7.8 m in the level flight stage. The maximum lift in different stages is shown in Table 5. At the same time, with the increase of separation, the influence of wake vortex on the lift variation of CRJ-900 aircraft is also decreasing.

Table 4: Emission data for CF34-8C5 engine at international (ISA).

Mode	Time (minute)	Power setting (%)	Fuel flow (kg/s)	Emission indices (g/kg)		
				HC	CO	NOx
Idle/Taxiing	26	7	0.064	0.13	18.25	4.6
Approach	4	30	0.179	0.06	4.24	10.75
Climb	2.2	85	0.53	0.02	0.57	12.6
Takeoff	0.7	100	0.648	0.02	0.64	14.69

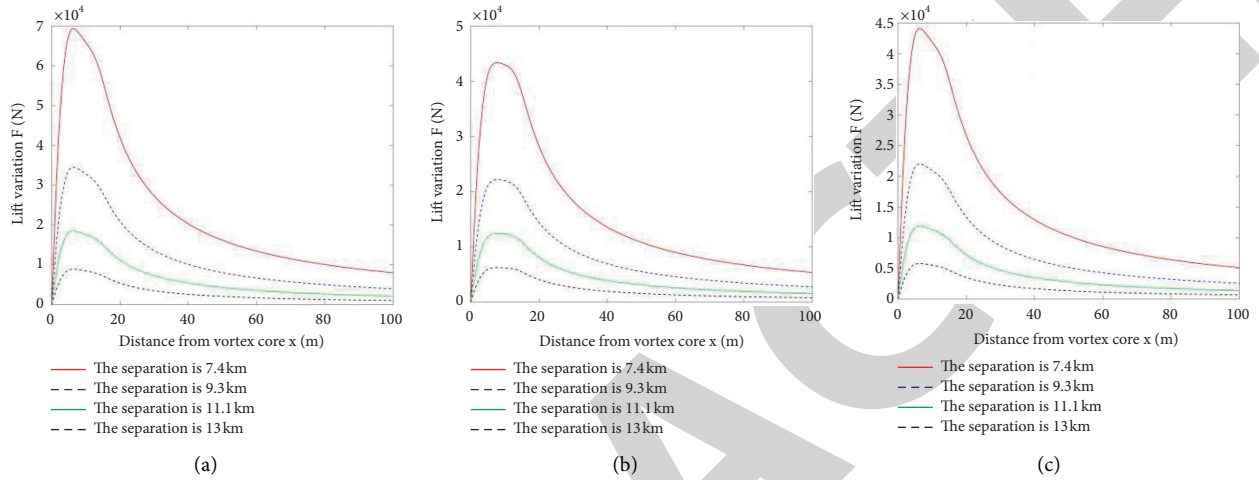

Figure 7: Variation curve of lift of a single wake vortex with the position of the aircraft from the vortex core. (a) Take off phase. (b) Level flight phase. (c) Landing phase.

Table 5: Variation of maximum lift of single vortex encountered in longitudinal direction.

Flight phase	Maximum lift position (m)	Maximum lift variation at different separation (N)			
		7.4	9.3	11.1	13
Takeoff	6.3	69286.24	34552.21	18545.81	8931.40
Level flight	7.8	43346.26	22158.85	12445.39	6253.04
Landing	6.3	44087.30	22046.42	11911.49	5804.20

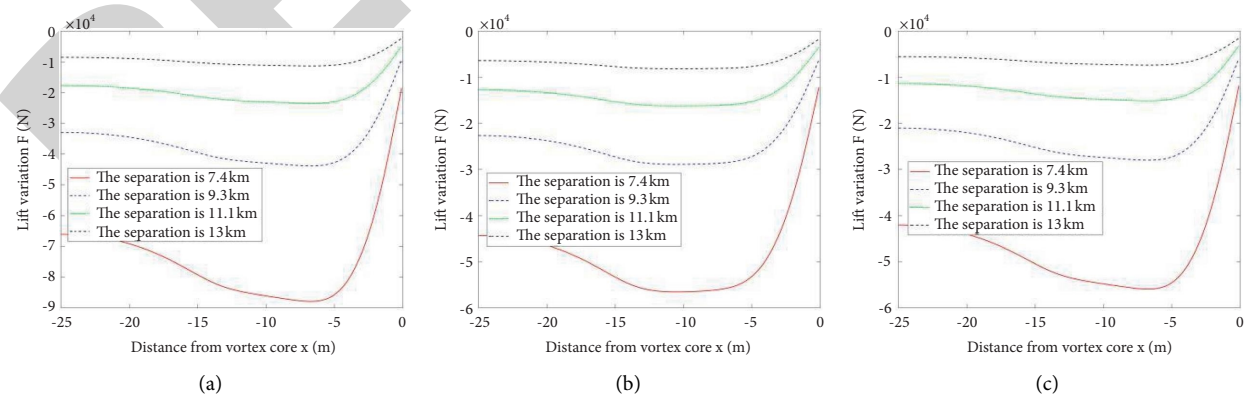

Figure 8: Variation curve of double vortex lift with aircraft distance from vortex core. (a) Takeoff phase. (b) Level flight phase. (c) Landing phase.

Table 6: Maximum lift variation of longitudinal encountering double vortices.

Flight phase	Maximum lift position (m)	Maximum lift variation at different separation (N)			
		7.4	9.3	11.1	13
Takeoff	−6.7	−87938.51	−43850.85	−23536.46	−11334.77
Level flight	−10.5	−55549.54	−28908.40	−16236.23	−8157.71
Landing	−6.7	−55954.09	−27979.31	−15116.82	−7366.06

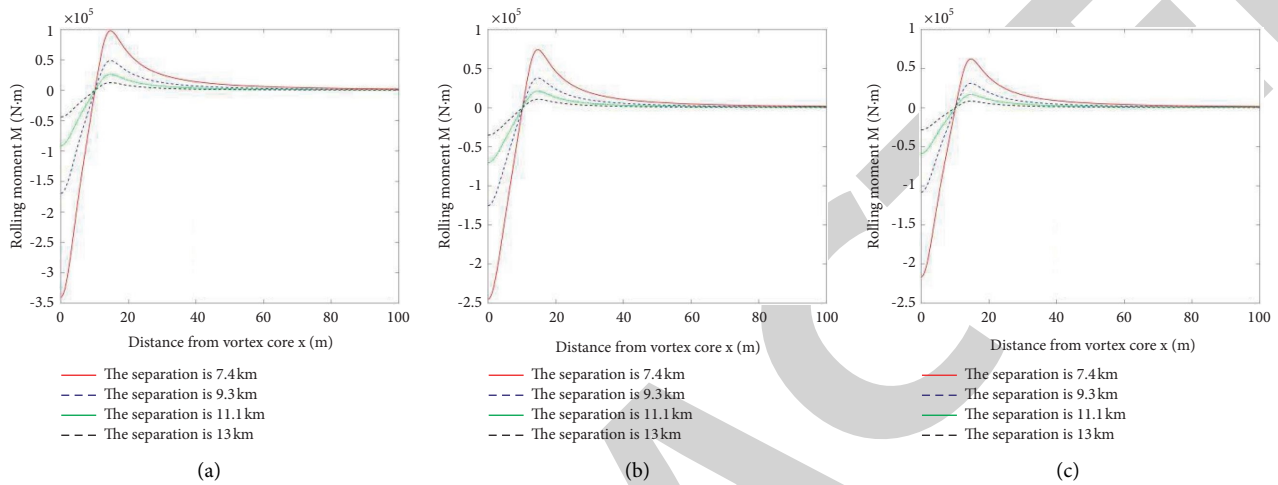

Figure 9: Variation of rolling moment when encountering a single wake vortex. (a) Takeoff phase. (b) Level flight phase. (c) Landing phase.

When the CRJ-900 aircraft longitudinally encounters the twin vortices of the front aircraft, the maximum lift variation is shown in Figure 8. In the takeoff and landing stages, the maximum position where the lift is generated is −6.7 m from the vortex core. When the aircraft moves outward from the vortex core position, the whole aircraft is subjected to the downwash force, the lift increases rapidly, and then begins to weaken and tend to be stable; in the level flight stage, due to the low air density and high cruise speed, the maximum lift position is −10.5 m from the vortex core. The maximum lift variation at different flight stages is shown in Table 6.

4.1.2. Rolling Moment Variation. The rolling moment of CRJ-900 aircraft longitudinally encountering the single vortex of the front aircraft is shown in Figure 9 and Table 7. At the vortex core, the maximum rolling moment will be generated due to the upper and lower washing forces on the wings on both sides. As the aircraft center is far away from the vortex core, the rolling moment gradually decreases, and then the torque direction changes. Finally, with the increase of distance, the force on the wings on both sides is stable; the rolling moment approaches zero.

The rolling moment of CRJ-900 aircraft longitudinally encountering the front double vortex is shown in Figure 10 and Table 8. At the same separation, the maximum rolling moment of CRJ-900 when encountering the double vortex wake is greater than that when encountering the single vortex. When the aircraft is 0 away from one side vortex core, the rolling moment is the largest. When it is on the center line of the two vortices, the forces on the wings on both sides are the same, so the rolling moment is reduced to 0.

4.1.3. Rolling Moment Coefficient. The rolling torque coefficient values in different flight stages are shown in Figures 11 and 12, and its variation law is roughly the same as that of rolling torque. At the center of the vortex core, due to the maximum rolling moment, the rolling moment coefficient of the wake vortex is also the maximum. As the aircraft center is far away from the center of the vortex core, its RMC value continues to decrease, and then the direction of the rolling moment changes, and the RMC value also changes from negative to positive.

According to relevant experiments under ICAO and RECAT-PWS-EU separation standards [31], the maximum value of rolling torque coefficient of heavy machine following medium-sized machine under reasonable worst case (RWC) is between 0.031 and 0.068. At the same time, the rolling moment coefficient control authority of the aircraft using ailerons is 0.05 to 0.07 [39]. As A380 is a super heavy aircraft, RMC of 0.031, 0.05, and 0.07 is selected as risk critical values to analyze its safety. It can be seen from Table 9 that the RMC value at the separation of 12 km is less than 0.05. Therefore, in the case of this example, it is safe to use the wake separation of the current super heavy aircraft following the medium-sized aircraft for CRJ-900 aircraft in different flight

Table 7: Variation of maximum rolling moment of single vortex encountered in longitudinal direction.

Flight phase	Maximum rolling moment position	Variation of maximum rolling moment at different separation			
		7.4	9.3	11.1	13
Takeoff	14.7	97718.75	48721.65	26150.03	12593.30
	0	−340145.25	−169594.98	−91025.73	−43836.10
Level flight	14.7	74058.84	37859.21	21263.39	10678.62
	0	−245234.25	−125364.87	−70410.40	−35274.49
Landing	14.7	62173.50	31086.72	16795.38	8183.92
	0	−216418.26	−108209.72	−58463.09	−28487.48

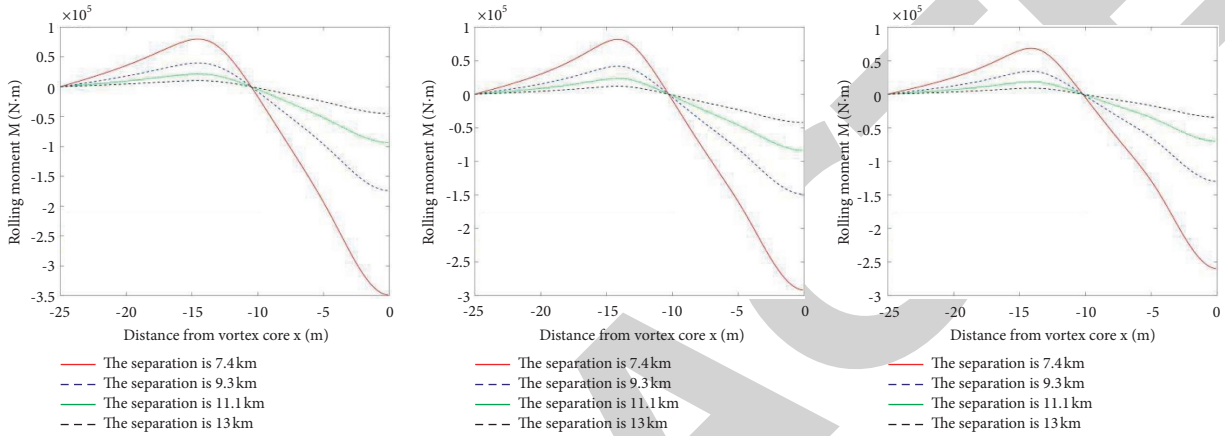

Figure 10: Variation of rolling moment in takeoff stage when encountering double vortex. (a) Takeoff phase. (b) Level flight phase. (c) Landing phase.

Table 8: Maximum value of double vortex rolling moment encountered.

Flight phase	Maximum position	Variation of rolling torque at different separation			
		7.4	9.3	11.1	13
Takeoff	−14.5	79753.67	39764.82	21342.73	10278.22
	0	−348878.42	−173949.19	−93362.73	−44961.55
Level flight	−14.2	81640.60	41735.04	23440.23	11777.28
	0	−291611.09	−149072.95	−83725.91	−42067.16
Landing	−14.1	68380.62	34181.28	18467.31	8998.62
	0	−259737.77	−129871.20	−70166.46	−34190.25

stages and has a large safety margin. Using the critical value of RMC, the safety critical separation of CRJ-900 aircraft is analyzed. The critical rolling moment and critical separation in different stages are shown in Table 10. When the critical value of RMC is 0.031, the maximum safety separation in different flight stages is 11960 m, which is reduced by 1040 m compared with the existing separation.

4.2. Transverse Encountering Front Wake Vortex

4.2.1. Force Variation of Aircraft. Taking the initial wake vortex circulation of A380 aircraft as an example, this paper calculates the position of the maximum up wash force and down wash force when CRJ-900 encounters the wake vortex laterally, and analyzes its stress under the wake vortex of different circulation. The distance through the vortex core and the stress of CRJ-900 are shown in Figure 13. The positions where CRJ-900 crosses the front turbine wake vortex and receives the maximum up washing force and down washing force are 13.6 m and 20.9 m through the vortex core, respectively. Since the maximum up washing force of the aircraft is greater than the maximum down washing force, the analysis of the most dangerous situation is mainly focused on the upwashing force.

4.2.2. Height Variation. As shown in the figure below, the variation of vortex height can be calculated according to the variation of vortex dissipation in different wake force stages, as shown in Figure 14.

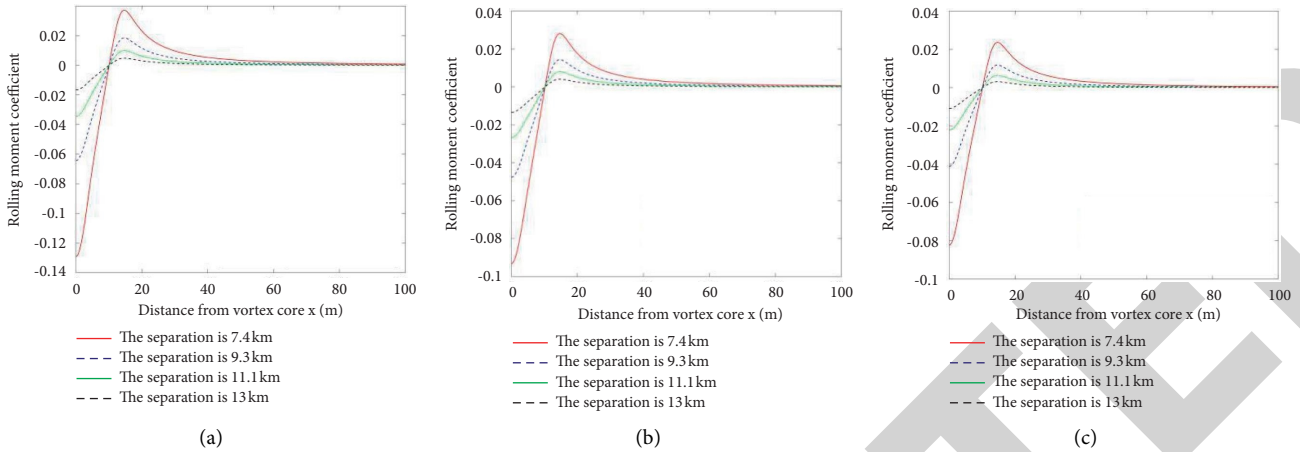

Figure 11: Variation of rolling moment coefficient with distance from vortex core when encountering single vortex. (a) Takeoff phase. (b) Level flight phase. (c) Landing phase.

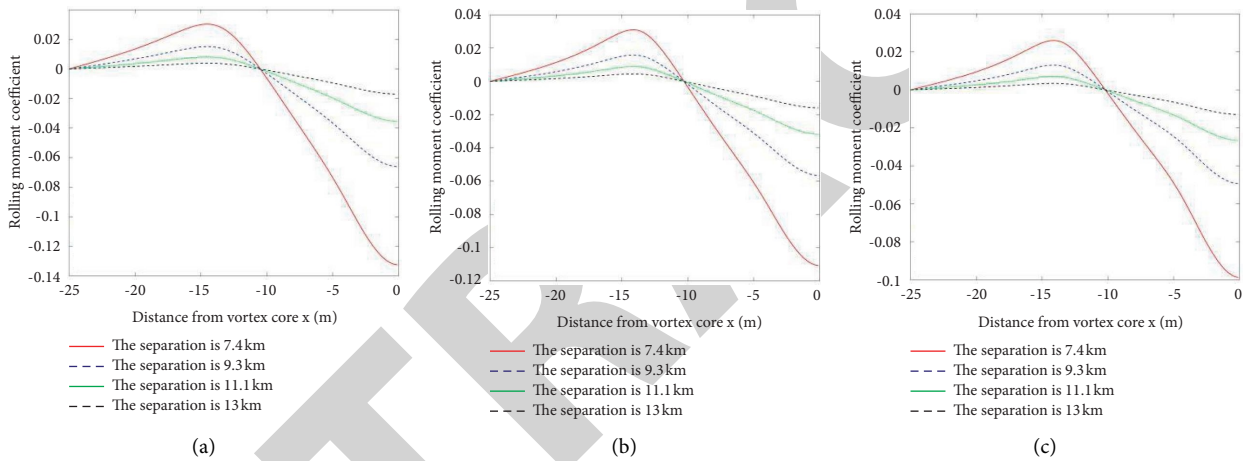

Figure 12: Variation of rolling moment coefficient with distance from vortex core when encountering double vortex. (a) Takeoff phase. (b) Level flight phase. (c) Landing phase.

Table 9: Maximum rolling moment coefficient.

Flight phase	Maximum position	Maximum rolling moment coefficient at different separation			
		7.4	9.3	11.1	13
Takeoff/single vortex	0	−0.1292	−0.0644	−0.0346	−0.0166
Level flight/single vortex	0	−0.0931	−0.0476	−0.0267	−0.0133
Landing/single vortex	0	−0.0821	−0.0411	−0.0222	−0.0108
Takeoff/twin vortex	0	−0.1325	−0.0661	−0.0355	−0.0171
Level flight/double vortex	0	−0.1107	−0.0398	−0.0318	−0.0160
Landing/double vortex	0	−0.0987	−0.0566	−0.0267	−0.0130

Table 10: Critical separation of different flight stages.

RMC threshold	Takeoff	Level flight	Landing
0.031	11960 m/ 149.5 s	11040 m/ 44.2 s	10820 m/ 152.4 s
0.05	10083 m/ 126.0 s	9075 m/36.3 s	10425 m/ 146.8 s
0.07	9021 m/112.8 s	8643 m/34.6 s	8868 m/124.9 s

4.2.3. Turbulence Intensity. According to the variation law of the maximum up wash force and down wash force with the wake vortex dissipation time, the variation law of the overload increment with the wake vortex dissipation in different flight stages is calculated.

Table 11 shows the classification of turbulence intensity by overload increment. When the aircraft suffers from moderate and above turbulence, it will produce difficult

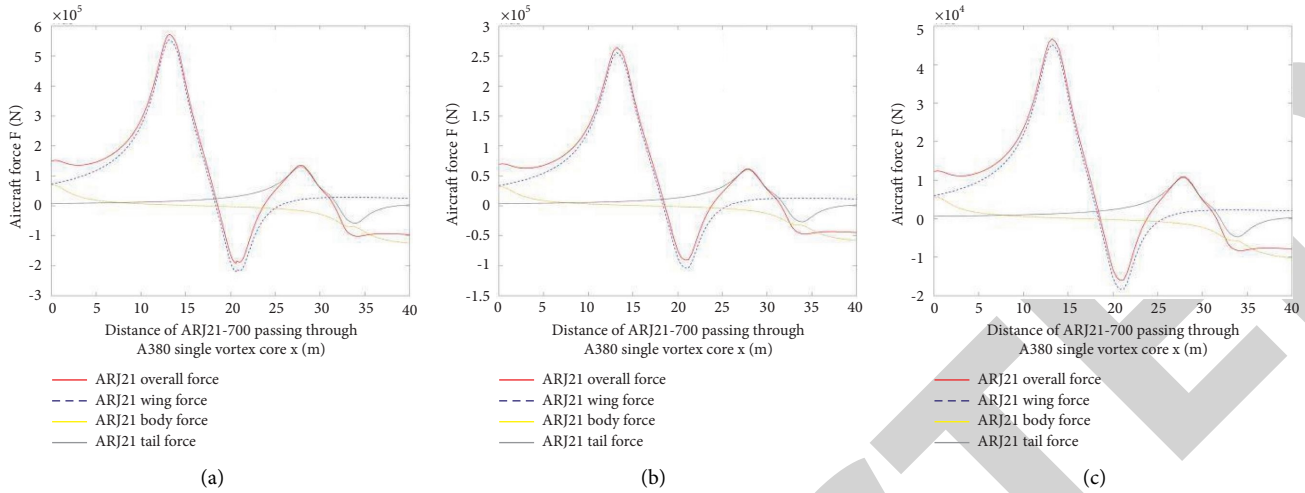

Figure 13: Stress diagram of CRJ900 across the front wake vortex. (a) Takeoff phase. (b) Level flight phase. (c) Landing phase.

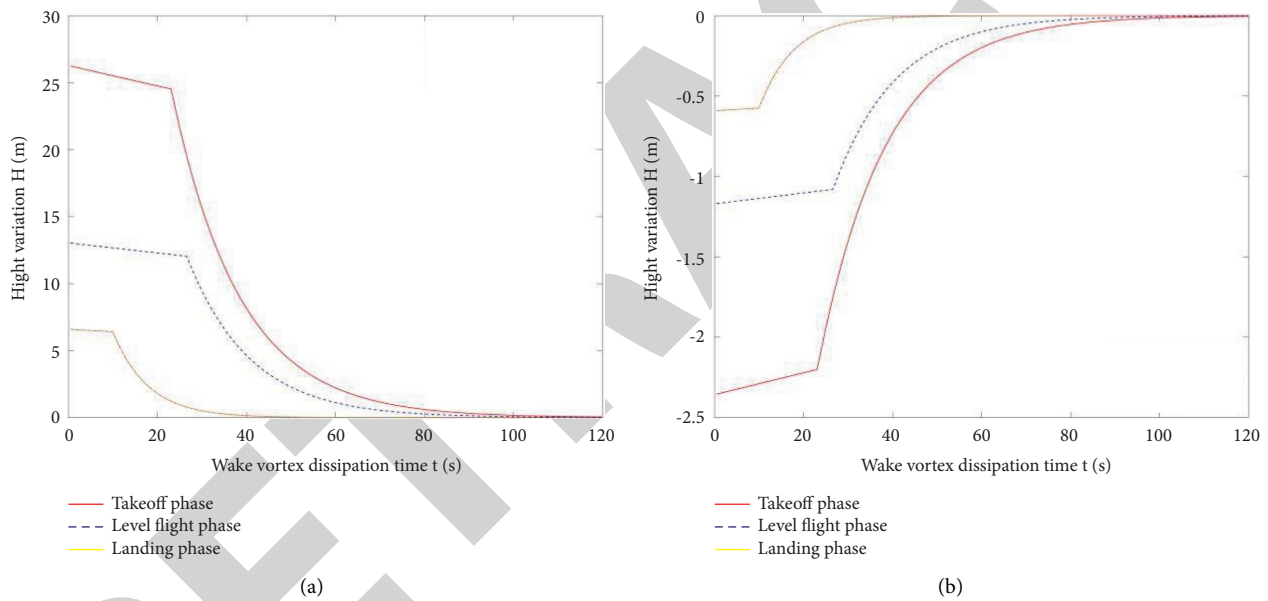

Figure 14: Schematic diagram of height variation of wake vortex before CRJ900 crossing. (a) Height change of maximum washing force. (b) Height change of maximum washing force.

Table 11: Classification of turbulence intensity corresponding to overload increment.

Turbulence intensity	Overload increment range
No turbulence	$\|\Delta n\| \le 0.15$
Mild turbulence	$0.15 < \|\Delta n\| \le 0.5$
Moderate turbulence	$0.5 < \|\Delta n\| \le 1.0$
Strong turbulence	$\|\Delta n\| \ge 1.0$

operation, abnormal instrument indication and other conditions; especially in the process of taking off and landing, it is easy to cause safety accidents when encountering more than moderate turbulence. As shown in Figure 15 above, under the condition of this example, the change of overload increment under the maximum washing force takes the overload increment as the critical value, the critical value in the takeoff stage is the wake vortex dissipation of 89.5 s, the level flight stage is 24.6 s, and the landing stage is 78.2 s.

4.3. Analysis of Pollutant Emission Reduction. The takeoff and landing phase is close to the safety separation calculated according to different RMC values. Through this separation value, the control separation time that can be reduced in each phase of the aircraft can be obtained. By bringing the reduced time into the LTO cycle, the reduction of fuel and pollutant emissions can be calculated, as shown in Table 12. When the RMC values are 0.031, 0.05, and 0.07 respectively,

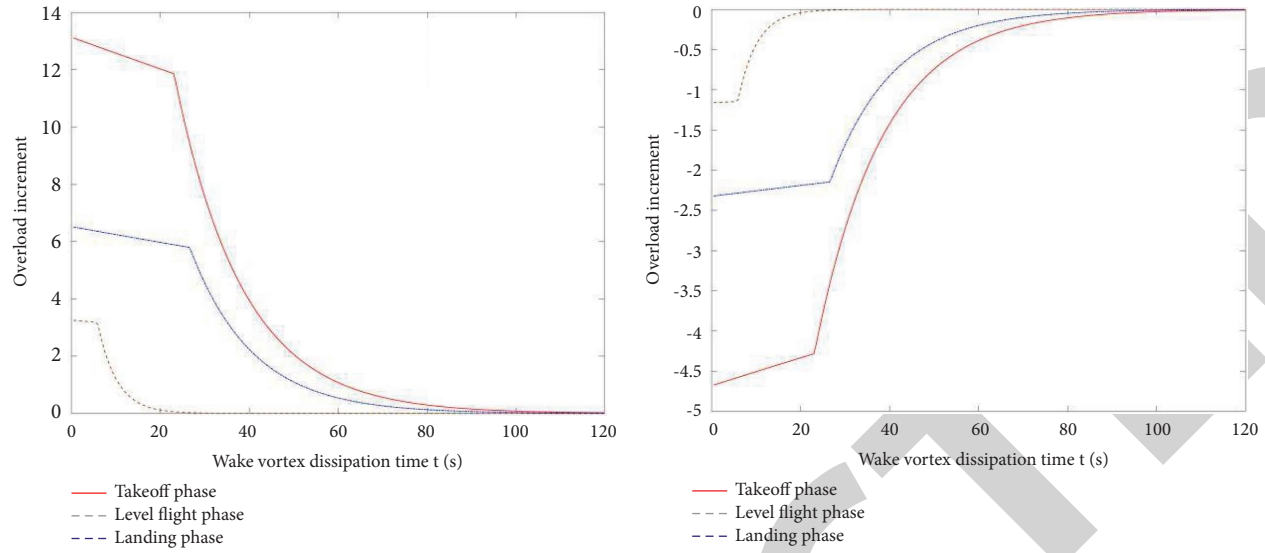

Figure 15: Schematic diagram of variation of wake vortex overload increment with wake vortex dissipation time before CRJ900 crossing. (a) Maximum up wash overload increment. (b) Maximum down wash overload increment.

Table 12: Fuel consumption and pollutant emission reduction under different RMC values.

RMC	Fuel consumption reduction (kg)	Fuel saving rate (%)	Pollutant emission reduction (g)			Pollutant emission reduction rate (%)
			HC	CO	NOx	
0.031	18.9	7.9	1.8	202.6	151.6	9.1
0.05	25.0	10.4	2.1	234.0	209.7	11.4
0.07	30.7	12.8	2.5	261.9	277	12.8

the fuel consumption can be reduced by 7.9%–12.8%, and the pollutant emission can be reduced by 9.1%–12.8%.

5. Conclusion

The front aircraft wake vortex dissipation and induced velocity model has been setup to analyze the dynamic response state of CRJ-900 aircraft encountering wake longitudinally and transversely at different flight stages and separation. The main research is as follows:

(1) An aerodynamic response model of wake encounter is optimized. For the front engine dissipation model, the influence of environmental parameters is added. According to the longitudinal and transverse encounter conditions, the strip method is introduced to establish different rear aircraft response models, calculate the wing, fuselage, and flat tail in sections, and then analyze the response states of CRJ-900 in different flight stages.

(2) Based on current safety indexes, it is verified that the wake separation standard is safe for the super heavy aircraft followed by medium-sized aircraft such as CRJ-900. Meanwhile, CRJ-900 aircraft has the potential to reduce the separation, for example, when the RMC critical value is 0.031, the critical distance of longitudinal encountering wake vortex is 11.94 km in takeoff stage, 11.04 km in level flight stage, and 10.82 km in landing stage. When encountering A380 wake vortex laterally, the safety critical time in takeoff stage is 89.5 s and that in landing stage is 78.2 s.

(3) An efficient air traffic operation could reduce aircraft fuel consumption and pollutant emission. Optimizing the control separation can shorten the waiting time of aircraft at the airport and in the air, allowing the reductions of fuel consumption and pollutant emission. For the critical safety separation calculated in this paper, fuel consumption can be reduced by 7.9%–12.8%, and pollutant emission can be reduced by 9.1%–12.8%.

Further research work needs to optimize the response model, verify it with simulator and flight experimental data, and establish a dynamic wake separation system to achieve the goal of improving control operation efficiency, energy conservation, and emission reduction.

Data Availability

Some or all data, models, or codes that support the findings of this study are available from the corresponding author upon reasonable request.

Conflicts of Interest

The authors declare that they have no conflicts of interest.

Acknowledgments

This work was supported by the National Natural Science Foundation of China (Grant no. U1733203), the Program of China Sichuan Science and Technology (Grant no. 2021YFS0319), the Special Project of Local Science and Technology Development Guided by the Central Government in 2020 (Grant no. 2020ZYD094), and the Civil Aviation Administration of China's safety capacity building project (Grant no. TM2019-16-1/3).

References

[1] S, C. Crow, "Stability theory for a pair of trailing vortices," *AIAA Journal*, vol. 8, no. 12, pp. 2172–2179, 1970.

[2] G, C. Greene, "An approximate model of vortex decay in the atmosphere," *Journal of Aircraft*, vol. 23, no. 7, pp. 566–573, 1986.

[3] J. A. Luton and S, A. Ragab, "The three-dimensional interaction of a vortex pair with a wall," *Physics of Fluids*, vol. 9, no. 10, pp. 2967–2980, 1997.

[4] T. Sarpkaya, "Decay of wake vortices of large aircraft," *AIAA Journal*, vol. 36, no. 9, pp. 1671–1679, 1998.

[5] T. Sarpkaya, "New model for vortex decay in the atmosphere," *Journal of Aircraft*, vol. 37, no. 1, pp. 53–61, 2000.

[6] T. Sarpkaya, R, E. Robins, and D, P. Delisi, "Wake-vortex eddy-dissipation model predictions compared with observations," *Journal of Aircraft*, vol. 38, no. 4, pp. 687–692, 2001.

[7] F. H. Proctor and J. Han, "Numerical study of wake vortex interaction with the ground using the terminal area simulation system," in *Proceedings of the 37th Aerospace Sciences Meeting and Exhibit*, p. 754, Reno,NV,U.S.A, January 1999.

[8] R. E. Robins, D. P. Delisi, and G. C. Greene, "Algorithm for prediction of trailing vortex evolution," *Journal of Aircraft*, vol. 38, no. 5, pp. 911–917, 2001.

[9] F. Holzäpfel, "Probabilistic two-phase wake vortex decay and transport model," *Journal of Aircraft*, vol. 40, no. 2, pp. 323–331, 2003.

[10] F. Holzäpfel, "Probabilistic two-phase aircraft wake-vortex model: further development and assessment," *Journal of Aircraft*, vol. 43, no. 3, pp. 700–708, 2006.

[11] F. Holzäpfel and M. Steen, "Aircraft wake-vortex evolution in ground proximity: analysis and parameterization," *AIAA Journal*, vol. 45, no. 1, pp. 218–227, 2007.

[12] F. Proctor, D. Hamilton, and G. Switzer, "TASS driven algorithms for wake prediction," in *Proceedings of the 44th AIAA Aerospace Sciences Meeting and Exhibit*, vol. 1073, Reno, NV, USA, January 2006.

[13] F. Proctor, N. Ahmad, G. Switzer, and F. L. Duparcmeur, "Three-phased wake vortex decay," in *Proceedings of the AIAA Atmospheric and Space Environments Conference*, p. 7991, Toronto, Ontario, Canada, August 2010.

[14] F. Proctor, N. Ahmad, and G. Switzer, "Crosswind shear gradient affect on wake vortices," in *Proceedings of the 3rd AIAA Atmospheric Space Environments Conference*, vol. 3038, Honolulu, Hl, USA, June 2011.

[15] C. Breitsamter, "Wake vortex characteristics of transport aircraft," *Progress in Aerospace Sciences*, vol. 47, no. 2, pp. 89–134, 2011.

[16] I. Hennemann and F. Holzäpfel, "Large-eddy simulation of aircraft wake vortex deformation and topology," *Proceedings of the Institution of Mechanical Engineers - Part G: Journal of Aerospace Engineering*, vol. 225, no. 12, pp. 1336–1350, 2011.

[17] I. De Visscher, T. Lonfils, and G. Winckelmans, "Fast-time modeling of ground effects on wake vortex transport and decay," *Journal of Aircraft*, vol. 50, no. 5, pp. 1514–1525, 2013.

[18] A. Stephan, F. Holzäpfel, and T. Misaka, "Aircraft wake vortex decay in ground proximity: physical mechanisms and artificial enhancement," *Journal of Aircraft*, vol. 50, no. 4, pp. 1250–1260, 2013.

[19] A. Stephan, F. Holzäpfel, and T. Misaka, "Hybrid simulation of wake-vortex evolution during landing on flat terrain and with plate line," *International Journal of Heat and Fluid Flow*, vol. 49, pp. 18–27, 2014.

[20] P. Weijun, L. Tian, K. Xianbiao, Z. Qingyu, and Z. Qiang, "Research progress of aircraft wake observation," *Journal of aerodynamics*, vol. 37, pp. 511–521, 2019.

[21] P. Weijun, W. Zhengyuan, and Z. Xiaolei, "Lidar aircraft wake vortex recognition based on K nearest neighbor," *Laser technology*, vol. 44, no. 04, pp. 471–477, 2020.

[22] D. Vicroy, P. Vijgen, H. Reimer, J. Gallegos, and P. Spalart, "Recent NASA wake-vortex flight tests, flow-physics database and wake-development analysis," in *Proceedings of the AIAA and SAE, 1998 World Aviation Conference*, p. 5592, Anaheim,CA,U.S.A, 1998 September.

[23] J. Kos, H. Blom, L. Speijker, M. B. Klompstra, and G. J. Bakker, "Probabilistic Wake Vortex Induced Accident Risk Assessment. Proceedings of usa/europe ATM R & D Symposium," 2000, https://reports.nlr.nl/bitstream/handle/10921/842/TP-2000-280.pdf?sequence=1.

[24] L. Speijker, A. Vidal, F. Barbaresco, M. Frech, H. Barny, and G. Winckelmans, "ATC-wake: integrated wake vortex safety and capacity system," *Journal of Air Traffic Control*, vol. 49, pp. 17–32, 2000.

[25] K. U. Hahn and C. W. Schwarz, "Safe limits for wake vortex penetration," in *Proceedings of the AIAA 2007 Guidance*, pp. 68–71, Navigation and Control Conference and Exhibit, 2007.

[26] L. Campos and J. Marques, "On an analytical model of wake vortex separation of aircraft," *Aeronautical Journal*, vol. 120, no. 1232, pp. 1534–1565, 2016.

[27] G. Van BarenVan Baren, V. Treve, F. Rooseleer, P. Van der GeestVan der Geest, and B. Heesbeen, "Assessing the severity of wake encounters in various aircraft types in piloted flight simulations," in *Proceedings of the AIAA Modeling and Simulation Technologies Conference*, vol. 1084, Grapevine, TX, USA, January 2017.

[28] Z. Zhaoning and Z. Bin, "Study on calculation method of longitudinal wake separation," *Journal of Civel Aviation University of China*, vol. 28, no. 05, pp. 10–12, 2010.

[29] F. Holzäpfel, L. Strauss, and C. Schwarz, "Assessment of dynamic pairwise wake vortex separations for approach and landing at Vienna airport," *Aerospace Science and Technology*, vol. 112, no. 2, 2021.

[30] P. Weijun, L. Yanan, L. Haijun, and Z. Sirui, "Study on wake vortex encounter and force model of open V-shaped runway," *Journal of safety and environment*, vol. 21, no. 03, pp. 1118–1124, 2021.

[31] S. V. Bohac, D. N. Assanis, and H. L. S. Holmes, "Speciated hydrocarbon emissions and the associated local ozone production from an automotive gasoline engine," *International Journal of Engine Research*, vol. 5, no. 1, pp. 53–70, 2004.

[32] L. Sherry, "Improving the accuracy of airport emissions inventories using disparate datasets," *IIE Transactions*, vol. 47, no. 6, pp. 577–585, 2015.
[33] A. Cook, G. Tanner, V. Williams, and G. Meise, "Dynamic cost indexing-managing airline delay costs," *Journal of Air Transport Management*, vol. 15, no. 1, pp. 26–35, 2009.
[34] V. V. Pham, J. Tang, S. Alam, C. Lokan, and H. A. Abbass, *Environmental Modelling & Software*, vol. 25, no. 12, pp. 1738–1753, 2010.
[35] U. Schumann, K. Graf, and H. Mannstein, "Potential to reduce the climate impact of aviation by flight level changes," in *Proceedings of the AIAA Atmospheric Space Environments Conference*, June 2011.
[36] P. Weijun, Y. Youjun, L. Xiaolin, Z. Qingyu, and L. Xin, "Calculation and analysis of new Taxiing modes on aircraft pollutant emissions in coastal airports of China," *Journal of Coastal Research*, no. 83, pp. 448–455, 2018.
[37] B. Jiang, Z. Yunfan, and Z. Chenglong L &Hao, "Simulation of optimal feeder airport runway structure for pollutant discharge control," *Journal of System Simulation*, no. 3, pp. 501–508, 2019.
[38] G. R Hough, "Remarks on vortex-lattice methods," *Journal of Aircraft*, vol. 10, no. 5, pp. 314–317, 1973.
[39] R. Luckner, "Modeling and simulation of wake vortex encounters: state-of-the-art and challenges," in *Proceedings of the AIAA Modeling and Simulation Technologies Conference*, p. 4633, Minneapolis, MN, USA, 2012, August.